Received 22 October 2024; revised 3 February 2025 and 25 March 2025; accepted 20 April 2025. Date of publication 23 April 2025; date of current version 9 May 2025. The review of this article was arranged by Editor S. Reggiani.

Digital Object Identifier 10.1109/JEDS.2025.3563644

High-Precision GaN-Based-SenseFET Design Based on a Lumped Parameter Electro-Thermal Network Model

XIAOTIAN TANG [1,2], QIMENG JIANG [1,2] (Member, IEEE), SEN HUANG [1,2] (Senior Member, IEEE), XINHUA WANG [1,2] (Member, IEEE), AND XINYU LIU [1,2]

1 High-Frequency High-Voltage Device and Integrated Circuits Research and Development Center, Institute of Microelectronics of Chinese Academy of Sciences, Beijing 100029, China
2 School of Integrated Circuits, University of Chinese Academy of Sciences, Beijing 100049, China

CORRESPONDING AUTHOR: Q. JIANG (e-mail: jiangqimeng@ime.ac.cn)

This work was supported in part by the National Key Research and Development Program of China under Grant 2022YFB3604400; in part by the Youth Innovation Promotion Association of Chinese Academy Sciences (CAS); in part by the CAS-Croucher Funding Scheme under Grant CAS22801; in part by the National Natural Science Foundation of China under Grant 62334012, Grant 62074161, Grant 62004213, Grant U20A20208, and Grant 62304252; in part by the University of CAS; and in part by IMECAS-HKUST-Joint Laboratory of Microelectronics.

ABSTRACT The lossless and accurate current sensing technology is highly desirable for feedback control, fast over-current protection, and diagnostics-prognostics development for high-frequency and high-efficiency power systems. The SenseFET technology, where a current sensor is monolithically integrated with a power transistor, has been widely used in power ICs due to its high precision and low cost. However, for a gallium nitride (GaN) lateral power device in multi-finger configurations, the non-uniform temperature distribution hinders its application in high-precision scenarios. This paper aims to address this issue through a design method of SenseFETs based on a lumped parameter electro-thermal network (LPETN) model. Based on the proposed model, the time-dependent temperature and conduction current distribution are obtained, and the optimized finger selection for the accurate current sense is performed. The thermal network part of the model is validated by the finite element method (FEM) results, and the electrical part is validated through LTSPICE simulation. Finally, taking a 50-finger GaN high electron mobility transistor (HEMT) device as an example, this model is used to select the fingers of a SenseFET for current sensing. Compared with the traditional method, the proposed approach significantly improves the accuracy of the SenseFET, which demonstrates its effectiveness.

INDEX TERMS SenseFETs, lumped parameter, electro-thermal network model, Gallium Nitride, power devices.

I. INTRODUCTION

Due to the material properties and device structure of gallium nitride (GaN) power devices, such as high critical electric field, high electron mobility and extremely low parasitic capacitance, the GaN-based power device has become the key technology for the next-generation power system featuring high conversion efficiency and high power density [1]. In a highly efficient power system, the current flowing through the switching device, i.e., GaN power device, should be monitored in real-time for control or protection [2], [3], [4]. For example, to achieve high-efficiency zero-voltage switching, a negative conduction current should be precisely monitored. In addition, over-current protection is another important feature to prevent degradation or burnout of the switching device [5], [6]. The traditional method of current sensing consists of placing a resistor in series with the sensed device [2]. This approach results in significant power loss, especially when the conduction current is high. Compared with the shunt resistor method, the SenseFET technology is a lossless approach to monitoring the power device current [7].

The SenseFET is a current sensing technology based on field-effect transistors, which acts as a current mirror to mimic

the transistor's conduction current [6], [8], [9], [10], [11]. The sensing accuracy is related to the placement of the sense fingers in the power array, since the temperature is not uniformly distributed across the whole power device. In addition, the non-uniform distribution of the temperature is dependent on time and/or mission profile [8], [12]. Therefore, to achieve accurate current detection, it is necessary to develop a time-dependent electro-thermal model for multi-finger GaN high electron mobility transistor (HEMT) devices to obtain accurate temperature distribution [13]. Based on the transient results of the electro-thermal model, the optimized placement for the sense finger is obtained.

In terms of electro-thermal models for power devices, various approaches have been proposed, including the analytical models, finite element method (FEM) models, and technology computer-aided design (TCAD) models [14], [15], [16], [17], [18], [19], [20]. Although the analytical models have high accuracy and fast computational algorithms, they have complex geometries and are difficult to integrate into circuit-level models. For the single-finger gate devices, the analysis can be performed accurately using TCAD simulation. However, for the multi-finger structure, the computational load is high and time-consuming. In general, the thermal distribution of the multi-finger devices can be determined through FEM models, but lacking thermal-electrical interaction.

Therefore, to deal with the above trade-off between functionality and calculation complexity, this paper proposes a lumped parameter electro-thermal network (LPETN) model, which can effectively perform fast electro-thermal coupling calculation. In addition, the calculated thermal distribution is consistent with the thermal simulation results of FEM, verifying its accuracy. In terms of electrical characteristics, this model can effectively characterize the current self-consistent process of multi-finger devices. Moreover, it can present the self-distribution effect of the current due to uneven heat distribution. Finally, based on this model, an optimal solution for the position of the SenseFET, which can guide the development of GaN power chips, is proposed.

The remainder of this paper is organized as follows. In Section II, the temperature stability issue of SenseFETs is mathematically analyzed, and a design method of finger selection is proposed. In Section III, a prototype of the SenseFET is presented with its test results. In Sections IV and V, a lumped parameter model for a 50-gate GaN HEMT device is developed, and its accuracy is verified through comparison with the FEM and SPICE models, which can be used for the subsequent finger selection. Section VI presents the results of the finger selection for SenseFETs using the LPETN model. Finally, the conclusions are drawn.

II. SENSEFET DESIGN

The SenseFET structure is embedded in the power device, as shown in Fig. 1(a). In order to achieve perfect matching of the conduction current, it is necessary to study the temperature distribution between the power fingers and the sensing fingers. The drain-source resistance of GaN devices varying at different temperatures, can be expressed as [21]:

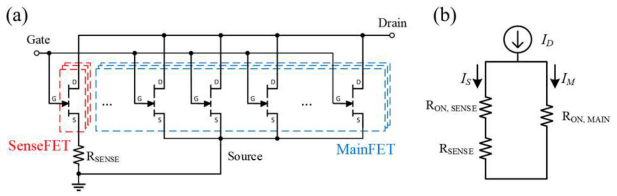

FIGURE 1. (a) Schematic and (b) equivalent electrical circuit of the proposed GaN-based SenseFET structure.

$$R_{DS(ON)} = R_{DS(ON)}{}^{25^\circ C} e^{(T-25^\circ C)/\eta} \tag{1}$$

where T is the device temperature and η is the thermal coefficient of the transistor.

The equivalent circuit is shown in Fig. 1(b), where the sensing module is connected in parallel with the power fingers. Since the SenseFET is connected in series with a sense resistor, the sensing current can be obtained by measuring the voltage across it. The current sensing factor (N_{SENSE}), based on the voltage drop across the sensing resistor, is the ratio between the main current and the sense current. Accordingly, the total current can be calculated using the current sensing factor. After considering the temperature effect, the current sensing factor can be expressed as:

$$\begin{aligned} N_{SENSE} &= \frac{I_M}{I_s} = \frac{R_s(TS) + R_{SENSE}}{RM(TM)} \\ &= \frac{R_s{}^{25^\circ C} e^{(TS-25^\circ C)/\eta}}{RM^{25^\circ C} e^{(TM-25^\circ C)/\eta}} + \frac{R_{SENSE}}{RM^{25^\circ C} e^{(TM-25^\circ C)/\eta}} \end{aligned} \tag{2}$$

where TM and TS represent the temperature of the mainFET and SenseFET, respectively. Since the SenseFET and the mainFET belong to the same HEMT device, it can be assumed that they have the same η value.

To alleviate the temperature dependence of N_{SENSE} in the switch, multiple parameters should be adjusted. In equation (2), the temperature dependence of the second term can be optimized by minimizing R_{SENSE}. Choosing a low-value sensing resistor is helpful for reducing the temperature dependence. In addition, due to thermal coupling, the temperature varies at different finger positions, leading to a temperature-dependent N_{SENSE}. Therefore, when selecting the SenseFET, the temperature bias should be carefully considered. In order to reduce the temperature dependence of the first term in equation (2), a specific finger can be selected as the SenseFET to compensate for the temperature inconsistency between the SenseFET and mainFET, which allows improving the accuracy of the current sensor. Based on this principle, this study proposes a high-precision SenseFET design method. The selection of the SenseFET is made using the LPETN model. The sensing accuracy can be improved by reducing the temperature bias between the SenseFET and mainFET.

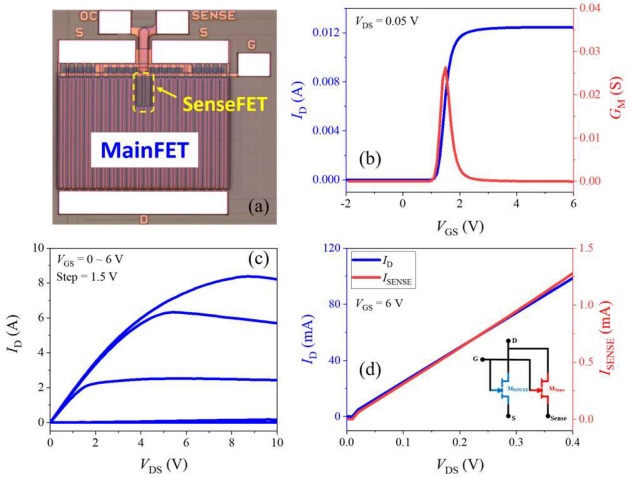

FIGURE 2. (a) Microscope picture of the fabricated SenseFET, (b) transfer, and (c) output characteristics of the power device. (d) The measured functionality of the SenseFET.

III. PROTOTYPE OF THE SENSEFET

In this work, to validate the functionality of the concept of SenseFETs, a prototype device was fabricated on a commercial 6-inch GaN-on-Si power device platform, as shown in Fig. 2(a). Fig. 2(b) and (c) show the measured transfer and output characteristics of the fabricated SenseFET device, where the power device has a *LGS*/*LG*/*LGD*/*W* of 1.5 μm/1.5 μm/22 μm/40 mm and the SenseFET part has a *LGS*/*LG*/*LGD*/*W* of 1.5 μm/1.5 μm/22 μm/500 μm. It is shown that the power device exhibits a *V*TH of +1.6 V from linear extrapolation, and a *R*ON of 0.55 Ω and a drain saturation current I_D of 8.4 A. The functionality of the SenseFET is also measured, as shown in Fig. 2(d), showing good current mirroring.

IV. THERMAL MODEL

A lumped parameter thermal network (LPTN) method is used for the thermal modeling and simulation of a SenseFET structure. The thermal network model is developed and simulated using MATLAB/Simulink.

A. LUMPED-PARAMETER THERMAL NETWORK MODEL

In this study, a 50-finger AlGaN/GaN HEMT is simulated, including a GaN layer on the top, an interlayer, a Si layer, an attachment layer, and a Cu base layer, as shown in Fig. 3(a). With respect to heat conduction, the AlGaN barrier layer is thin enough to be negligible, and therefore it is omitted from this model. In addition, the source and drain regions of the device are thermally neglected. The structural parameters of this simulation model are listed in Table 1.

Fig. 3(b) illustrates the two dimensional cross section of the structure divided into many blocks by dashed lines. Several parts inside the case, including the interface layer, attachment layer, and bottom Cu layer, are represented by the interlayer. For the horizontal grid, there is one block below the gate finger, and three identical blocks between

TABLE 1. Parameters of the simulation model.

Parameter	Value	Unit
Gate length (L_g)	2	μm
Gate width (W_g)	1	mm
Gate-to-Gate spacing (L_{gg})	40	μm
Total length of geometry (L_{total})	4	mm
Number of fingers (n)	50	-
GaN thickness (t_{GaN})	2	μm
Interlayer thickness (t_{inter})	1	μm
Substrate thickness (t_{sub})	200	μm
Reference temperature (T_a)	300	K

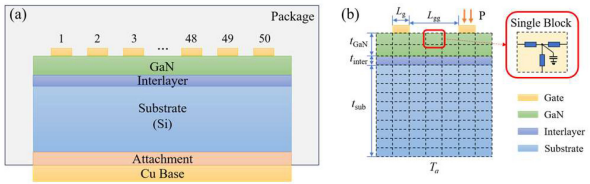

FIGURE 3. (a) Cross section of a 50-finger GaN HEMT and (b) part of the LPTN model.

the two gate fingers. The leftmost and rightmost regions of the structure are divided into 8 blocks whose lengths exponentially increase. For the vertical grid, the GaN layer is replaced by two layers of blocks with layers having a thickness of 1 μm each, and the interlayer contains one layer. The Si layer is represented by ten layers of blocks, and each layer has a thickness of 20 μm. To simplify the representation, only two fingers of the HEMT structure are shown in Fig. 3(b). Accordingly, the whole HEMT structure is partitioned into 213 grids per row and 13 grids per column. Experimental verification showed that further increasing the number of elements has a minimal impact on the results.

Considering only two-dimensional heat transfer, each block is defined by a node, two thermal resistances, and a thermal capacitance. The thermal capacitance of each element is connected between the node and a thermal ground. The transverse and longitudinal thermal resistances represent the transverse and longitudinal heat conduction, respectively. The thermal capacitance represents the heat storage capacity. The values of the thermal resistances and the thermal capacitance of each element can be determined by the material and the element size. The thermal resistance (*R*th) can be expressed as:

$$R_{\text{th}} = \frac{L}{k \times A}, \tag{3}$$

and the thermal capacitance (*C*th) can be expressed as:

$$C_{\text{th}} = c_p \times L \times A \tag{4}$$

where k is the thermal conductivity, c_p is the volumetric heat capacity, L is the length of the heat flow path, and A is the area normal to the heat flow path. After calculating *R*th and *C*th, we can obtain the transient temperature at each node using the following equation:

$$T(t) = P \times R\text{th}(1 - \exp(-t/\tau)) \tag{5}$$

where $\tau = R\text{th} \times C\text{th}$.

TABLE 2. Parameters of the material.

Material Parameters	GaN	Si
Thermal conductivity ($W \cdot m^{-1} \cdot K^{-1}$)	160	148
Specific heat capacity ($J \cdot kg^{-1} \cdot K^{-1}$)	490	700
Density ($kg \cdot m^{-3}$)	6070	2330
Volumetric heat capacity ($J \cdot m^{-3} \cdot K^{-1}$)	2.97e6	1.63e6

The parameters of the material used in this paper are presented in Table 2. Thus, the values of the thermal resistance and thermal capacitance can be determined by calculation. As a result, the HEMT is translated into a lumped parameter thermal network.

In the equivalent thermal network, current represents power, and voltage represents node temperature. Therefore, the top contacts inject currents corresponding to the dissipated power density at the gate finger node. The voltage sources and thermal grounds are connected in series at the bottom of the thermal network, and their value is equal to the ambient temperature (T_a). The remaining surfaces are considered adiabatic. The temperature value can then be obtained by detecting the voltage of each node.

Based on the datasheet of the commercial device GaN system (065-011-1-L) [21], the thermal resistance from the device junction to the case (R_{jc}) is set to 1.4 K/W. Therefore, by adjusting the thermal resistance of the interlayer, the overall thermal resistance of the thermal network is set to 1.4 K/W. In this section, the power input of each gate finger is fixed at 1.8 W. Since the network is two-dimensional planar, the input power density is 1800 W/m. The ambient temperature (T_a) is set to 300 K.

B. THERMAL MODEL VALIDATION THROUGH FEM RESULTS

An FEM simulation was conducted using the COMSOL Multiphysics software for the abovementioned identical HEMT structure. In COMSOL, the physics module 'Heat Transfer in Solids' was selected. The heat flux type was then selected as "heat rate", and the value was set to 1.8 W per finger. A fixed temperature of 300 K was set on the bottom surface. The geometry was then meshed with approximately 65,600 nodes and 127,000 triangular elements.

Fig. 4 compares the surface temperature profiles and finger temperatures obtained by LPTN and FEM simulations. It can be seen that the gate finger temperature result of LPTN model is very close to that of the FEM simulation, with an error of about 2.4%. For the nodes between the gate fingers, the temperature results are consistent. The temperatures of the geometric region outside the outermost grid fingers are also consistent. The two-dimensional temperature distributions obtained by the LPTN model and FEM simulation are shown in Fig. 5. The color bars of the two figures are identical. This result further indicates that the LPTN model for the entire structure's temperature simulation is nearly identical to the FEM simulation.

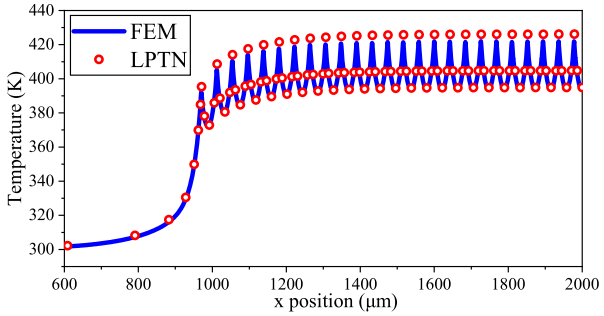

FIGURE 4. Comparison between the finger temperatures of the LPTN model and FEM.

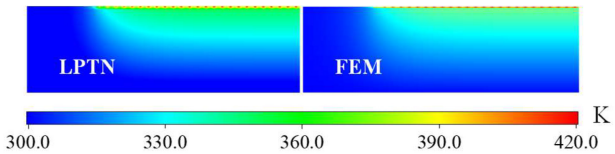

FIGURE 5. Temperature profiles of the LPTN model (with a 3% bias) and FEM.

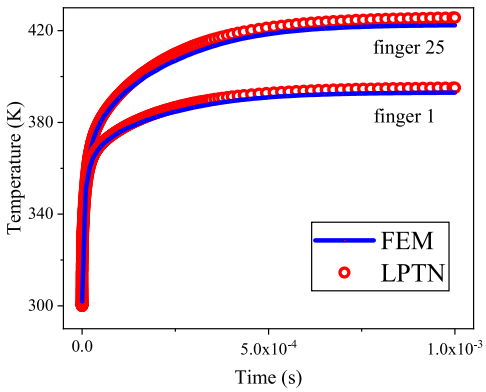

FIGURE 6. Comparison between the transient temperatures of finger 1 and finger 25.

This result demonstrates the consistency of the steady-state simulation, indicating that the thermal resistance values in the thermal network were correctly set. For the transient simulations, the results from the two models were compared for the 1st and 25th gate fingers. Fig. 6 shows that the transient temperature results are also consistent. In summary, the consistency with the FEM results shown in Figs. 4-6 indicates that the proposed simple approach can predict both the static and dynamic thermal behavior of multi-finger HEMT structures. Notably, no fitting parameter were used in the model.

V. SELF-CONSISTENT ELECTRO-THERMAL MODEL

In this section, the proposed electro-thermal model is first validated through LTSPICE simulation. The LPETN model, including a constant current source, is then developed for the SenseFETs design.

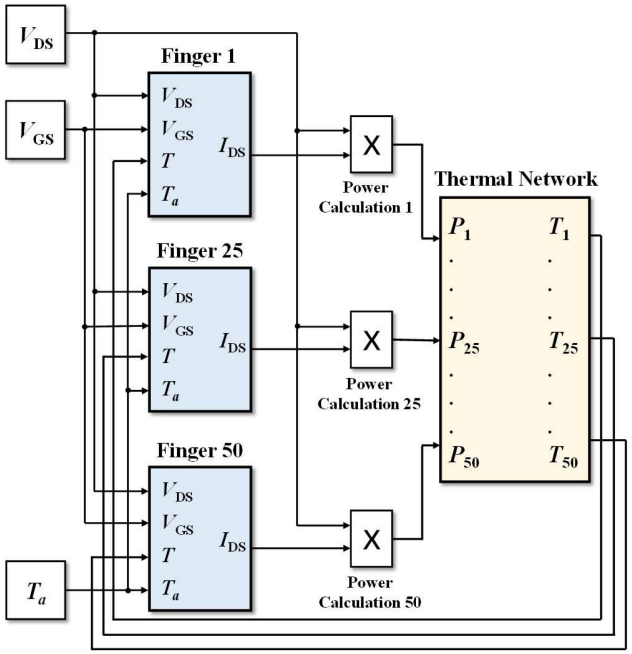

FIGURE 7. Schematic representation of the LPETN model for a constant voltage source.

TABLE 3. Parameters of the electro-thermal model.

Parameter	Value	Parameter	Value
A_1	0.0322	B_1	0.05263
A_2	0.147	B_2	0.94376
A_3	30.83459808	B_3	10.58e-3
A_4	1.7	B_4	-0.004
x_0	1.1	B_5	130e-3
x_1	0.3	B_6	2.725
x_2	1.0		

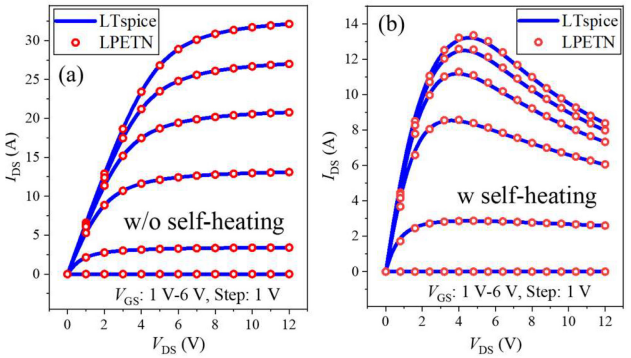

FIGURE 8. Comparison between the output curves (a) at ambient temperature of 300 K and (b) coupled with temperature.

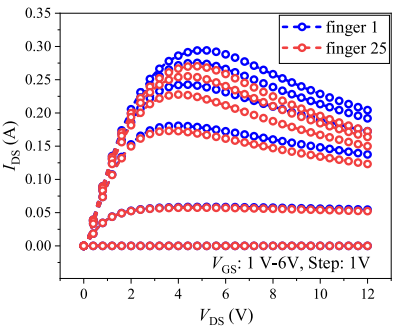

FIGURE 9. The output curves of finger 1 and finger 25 using the LPETN model.

A. ELECTRO-THERMAL MODEL VALIDATION THROUGH LTSPICE RESULTS

In this study, the temperature-dependent model of GS-065-011-1-L [21] is used as the electrical model. The used drain current model is given by:

$$I(V_{\rm DS}, V_{\rm GS}, T, T_a) = A_1 \times (-(T - T_a) \times A_2 + A_3) \times \log\left(1 + e^{26\times(V_{\rm gs} - A_4)}\right) \times \frac{V_{\rm ds}}{1 + \max\left(x_0 + x_1 \times (V_{\rm gs} + x_2), 0.2\right) \times V_{\rm ds}} \quad (6)$$

$$V_{\rm gs} = V_{\rm GS} - I \times R_{\rm s} \quad (7)$$

$$V_{\rm ds} = V_{\rm DS} - I \times (R_{\rm s} + R_{\rm d}) \quad (8)$$

$$R_{\rm s} = B_1 \times \left(B_3 \times (1 - 1 \times B_4 \times (T - T_a)) + B_5 \times \left(\frac{T}{T_a}\right)^{B_6}\right) + 10^{-4} \quad (9)$$

$$R_{\rm d} = B_2 \times \left(B_3 \times (1 - 1 \times B_4 \times (T - T_a)) + B_5 \times \left(\frac{T}{T_a}\right)^{B_6}\right) + 10^{-4} \quad (10)$$

where T is the channel temperature, T_a is the ambient temperature, $V_{\rm GS}$ is the gate-source voltage, $V_{\rm DS}$ is the drain-source voltage, $R_{\rm s}$ is the source resistance, and $R_{\rm d}$ is the drain resistance. The parameters of the model are presented in Table 3, which are extracted from the SPICE model of the GS-065-011-1-L device.

The electrical model of the HEMT device is coupled with the thermal network model described in Section IV, as shown in Fig. 7. Power dissipation of each finger in the electrical model is obtained by multiplying output current ($I_{\rm DS}$) by drain voltage ($V_{\rm DS}$). It is then used as the input for the thermal network. The temperature of each finger calculated by the thermal network is subsequently fed back to the electrical model, as expressed in equations (6)–(10). The initial value of T is set to 300 K. After iterations, the output characteristics curve of the device can be obtained, as shown in Fig. 8. Fig. 8(a) (dotted line) shows the output characteristics obtained by the LPETN model at a fixed temperature of 300 K, while Fig. 8(b) (dotted line) shows the curve with self-heating effects. To validate the electro-thermal model, electrical properties were simulated in LTSPICE using the SPICE model available on the GaN system website. The LTSPICE results are shown in Fig. 8(a) and (b) (solid line). The two sets of data are highly consistent with each other, indicating the accuracy of the proposed electro-thermal coupling model. Fig. 9 shows that different fingers are affected by temperature in varying degrees, resulting in different self-heating effects on their output characteristics curves. The proposed electro-thermal model can determine the electrical characteristics of each finger,

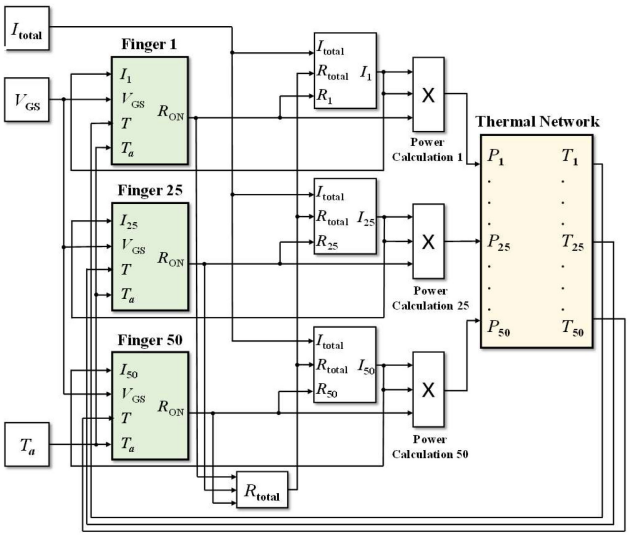

FIGURE 10. Schematic representation of the LPETN model for a constant current source.

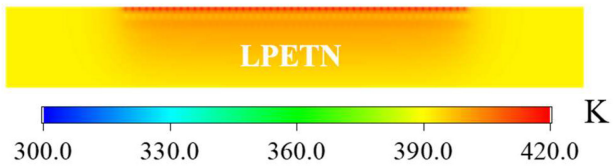

FIGURE 11. Temperature distribution of the LPETN model.

significantly reducing computational cost and simulation time compared to other methods, which is due to the use of the LPTN model.

B. ELECTRO-THERMAL MODEL FOR SENSEFETs DESIGN

The electrical model given above is used under a constant voltage source. However, the input of the device is usually equivalent to a constant current source in an actual circuit. Therefore, the variation of the on-resistance (RON) with VGS, I_{DS}, and T, is derived from equations (6)–(10):

$$R_{ON}(I, V_{GS}, T, T_a) = R_{ds} + R_s + R_d \tag{11}$$

$$R_{ds} = \frac{1}{A_1 \times (-(T - T_a) \times A_2 + A_3) \times \log\left(1 + e^{26\times(Vgs - A_4)}\right) - \max\left(x_0 + x_1 \times (V_{gs} + x_2), 0.2\right) \times I} \tag{12}$$

The variation of the on-resistance with temperature can be determined using equation (11). All the gate fingers are connected in parallel. Based on Kirchhoff's law, the current of each finger gate can be calculated for a constant total current. The power of each finger is calculated as I^2R and used as input to the thermal network in order to compute the finger temperatures which will be fed back into the electrical model. To better simulate the actual device, the environmental thermal resistance is added to the thermal network. The ambient thermal resistance is set to 5 K/W. Accordingly, the thermal resistance of the entire thermal network (R_{ja}) is 6.4 K/W, which corresponds to

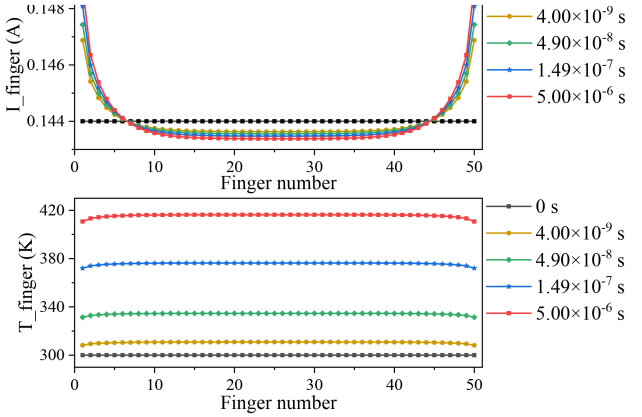

FIGURE 12. Current and temperature variation with time for each finger.

the datasheet. Fig. 10 shows the schematic diagram of the electro-thermal model for a constant current source, which is used for the SenseFET-based current sensor in the following section.

VI. OPTIMIZED DESIGN OF SENSEFETs

The LPETN model of a constant current source was used to simulate a 50-finger gate GaN HEMT device. Fig. 11 shows the temperature distribution of the device, which increases due to thermal transfer from its bottom to the environment. As a result, the on-resistance of the device significantly increases with temperature. Fig. 12 shows the changes in current and temperature of each finger over time. As the temperature increases, the current distribution between the parallel fingers becomes non-uniform. The middle finger has higher temperature and larger on-resistance, which results in a lower current compared with the average one. After iterations, a temperature difference of 6 K and a current difference of 4% were obtained between finger 1 and finger 25. As the temperature difference increases, the current difference also increases. Therefore, the traditional SenseFET experiences a significant increase in error due to temperature differences.

In general, increasing the number of fingers improves the stability and matching of the SenseFET, but also increases power loss and cost. Therefore, optimization and trade-off are necessary. In this paper, 1, 2, and 3 fingers were considered as a SenseFET to characterize the tracking relationship between the sense current (I_{SENSE}) and the drain current (ID). Based on the simulation results of the electro-thermal model, the fingers having the smallest error were selected as a SenseFET for higher accuracy, as shown in Fig. 13(a). For one finger, the algorithm selected finger 7 as the SenseFET, with an error of 0.058% between the $I_{SENSE} \times N_{SENSE}$ and ID. For two fingers, finger 5 and finger 41 were chosen as SenseFET, with an error of 0.0057%. When finger 6, finger 8, and finger 45 were selected as a three-finger SenseFET, the error was 0.00021%. The traditional finger selection method, which selects the edge or middle finger as a SenseFET, was compared with the proposed method, as

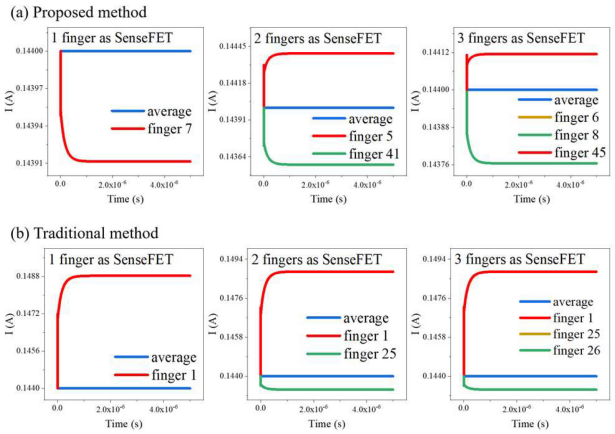

FIGURE 13. Comparison between the SenseFET finger selection of the (a) proposed and (b) traditional methods.

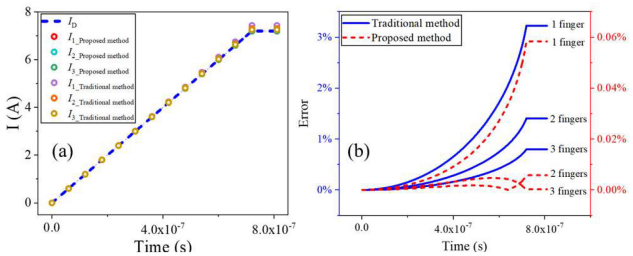

FIGURE 14. Comparison between the results of (a) current following and (b) sensing error with different numbers of fingers obtained by the proposed and traditional methods.

shown in Fig. 13(b). The errors of the 1-finger (finger 1), 2-finger (finger 1 and finger 25), and 3-finger (fingers 1, 25, and 26) SenseFETs in the traditional method were 3.2, 1.4, and 0.8%, respectively. The optimization effect of SenseFETs with different numbers of fingers is shown in Fig. 14(a). A comparison between the sensing errors is shown in Fig. 14(b). It can be seen that the error of the optimized SenseFET was significantly reduced. This indicates that the SenseFET designed based on the proposed model can effectively improve the current sensing accuracy, making it suitable for high-precision current detection applications such as in DC-DC converters. In addition, compared to the traditional method, the computational cost of the proposed method is negligible. Therefore, the simulation using this model can assist in selecting SenseFETs during the device design stage, facilitating the subsequent layout design.

VII. CONCLUSION

This paper studies a GaN SenseFET technology which can be easily implemented due to the lateral configuration of the GaN power device. A lumped parameter electro-thermal network model is used to achieve an accurate current sensing of multiple-finger GaN power FETs. A two-dimensional physical-level lumped parameter thermal network model is developed to determine the temperature distribution at each gate finger. The accuracy of the thermal network is verified through FEM results. The thermal network is then coupled with the electrical model to simulate the real-time variation of gate finger current with temperature. The reliability of the electro-thermal coupled model is validated through LTSPICE results. Finally, it is demonstrated that the accuracy of the SenseFET obtained by this optimization method is significantly improved compared with that of the traditional method. Therefore, the proposed approach can be considered a high-precision current measurement method for GaN power devices.

REFERENCES

[1] K. J. Chen et al., "GaN-on-Si power technology: Devices and applications," *IEEE Trans. Electron Devices*, vol. 64, no. 3, pp. 779–795, Mar. 2017, doi: 10.1109/TED.2017.2657579.

[2] S. Ziegler, R. C. Woodward, H. H.-C. Iu, and L. J. Borle, "Current sensing techniques: A review," *IEEE Sens. J.*, vol. 9, no. 4, pp. 354–376, Apr. 2009, doi: 10.1109/JSEN.2009.2013914.

[3] M. E. Ibrahim and A. M. Abd-Elhady, "A proposed non-invasive Rogowski coil design for measuring 3-phase currents through a 3-core cable," *IEEE Sens. J.*, vol. 21, no. 1, pp. 593–599, Jan. 2021, doi: 10.1109/JSEN.2020.3012839.

[4] C. Guo, H. Zhang, H. Guo, L. Chen, W. Chen, and N. Yu, "Crosstalk analysis and current measurement correction in circular 3D magnetic sensors arrays," *IEEE Sens. J.*, vol. 21, no. 3, pp. 3121–3133, Feb. 2021, doi: 10.1109/JSEN.2020.3028149.

[5] R. Sun, Y. C. Liang, Y.-C. Yeo, Y.-H. Wang, and C. Zhao, "Realistic trap configuration scheme with fabrication processes in consideration for the simulations of AlGaN/GaN MIS-HEMT devices," *IEEE J. Emerg. Sel. Top. Power Electron.*, vol. 4, no. 3, pp. 720–729, Sep. 2016, doi: 10.1109/JESTPE.2016.2549959.

[6] R. Sun, Y. C. Liang, Y.-C. Yeo, and C. Zhao, "Au-free AlGaN/GaN MIS-HEMTs with embedded current sensing structure for power switching applications," *IEEE Trans. Electron Devices*, vol. 64, no. 8, pp. 3515–3518, Aug. 2017, doi: 10.1109/TED.2017.2717934.

[7] H. P. Forghani-Zadeh and G. A. Rincon-Mora, "Current-sensing techniques for DC-DC converters," in *Proc. 45th Midwest Symp. Circuits Syst. (MWSCAS)*, Tulsa, OK, USA, 2002, pp. II-577–II-580, doi: 10.1109/MWSCAS.2002.1186927.

[8] M. Biglarbegian and B. Parkhideh, "Characterization of SenseGaN current-mirroring for power GaN with the virtual grounding in a boost converter," in *Proc. IEEE Energy Convers. Congr. Exposit. (ECCE)*, Cincinnati, OH, USA, Oct. 2017, pp. 5915–5919, doi: 10.1109/ECCE.2017.8096977.

[9] V.-S. Nguyen, R. Escoffier, S. Catellani, M. FaYolle-Lecocq, and J. Martin, "Design, implementation and characterization of an integrated current sensing in GaN HEMT device by using the current-mirroring technique," in *Proc. 24th Eur. Conf. Power Electron. Appl. (EPE ECCE Europe)*, 2022, pp. 1–10. [Online]. Available: https://ieeexplore.ieee.org/document/9907646

[10] M. S. Zaman et al., "Integrated SenseHEMT and gate-driver on a 650-V GaN-on-Si platform demonstrated in a bridgeless totem-pole PFC converter," in *Proc. 32nd Int. Symp. Power Semicond. Devices ICs (ISPSD)*, Vienna, Austria, Sep. 2020, pp. 26–29, doi: 10.1109/ISPSD46842.2020.9170100.

[11] M. Basler, R. Reiner, S. Moench, P. Waltereit, R. Quay, and J. Haarer, "Compact GaN power ICs with power HEMT, gate driver, temperature sensor, current sense-FET and amplifier," in *Proc. 35th Int. Symp. Power Semicond. Devices ICs (ISPSD)*, May 2023, pp. 191–194, doi: 10.1109/ISPSD57135.2023.10147498.

[12] R. Germana, "Power mos current sensefet temperature drift study and improvement by the help of 3D simulations," in *Proc. 24th Int. Symp. Power Semicond. Devices ICs*, Bruges, Belgium, Jun. 2012, pp. 413–416, doi: 10.1109/ISPSD.2012.6229109.

[13] L. Wu and M. Saeedifard, "A simple behavioral electro-thermal model of GaN FETs for SPICE circuit simulation," *IEEE J. Emerg. Sel. Top. Power Electron.*, vol. 4, no. 3, pp. 730–737, Sep. 2016, doi: 10.1109/JESTPE.2016.2574329.

[14] E. R. Heller and A. Crespo, "Electro-thermal modeling of multifinger AlGaN/GaN HEMT device operation including thermal substrate effects," *Microelectron. Rel.*, vol. 48, no. 1, pp. 45–50, Jan. 2008, doi: 10.1016/j.microrel.2007.01.090.

[15] A. B. Jorgensen, S. Munk-Nielsen, and C. Uhrenfeldt, "Overview of digital design and finite-element analysis in modern power electronic packaging," *IEEE Trans. Power Electron.*, vol. 35, no. 10, pp. 10892–10905, Oct. 2020, doi: 10.1109/TPEL.2020.2978584.

[16] E. Catoggio, S. D. Guerrieri, and F. Bonani, "Efficient TCAD thermal analysis of semiconductor devices," *IEEE Trans. Electron Devices*, vol. 68, no. 11, pp. 5462–5468, Nov. 2021, doi: 10.1109/TED.2021.3076753.

[17] A. Dey, N. Shafiei, R. Khandekhar, W. Eberle, and R. Li, "Lumped parameter thermal network modelling of power transformers," in *Proc. 20th IEEE Intersoc. Conf. Thermal Thermomech. Phenomena Electron. Syst. (iTherm)*, San Diego, CA, USA, Jun. 2021, pp. 172–178, doi: 10.1109/ITherm51669.2021.9503171.

[18] M. Tang, L. Chen, B. Li, H. Yue, Y. Tang, and J. Mao, "Nonlinear thermal analysis of AlGaN/GaN HEMTs with temperature-dependent parameters," *IEEE Trans. Electron Devices*, vol. 68, no. 9, pp. 4565–4570, Sep. 2021, doi: 10.1109/TED.2021.3097707.

[19] J. Li, M. Tang, and J. Mao, "Analytical thermal model for AlGaN/GaN HEMTs using conformal mapping method," *IEEE Trans. Electron Devices*, vol. 69, no. 5, pp. 2313–2318, May 2022, doi: 10.1109/TED.2022.3162167.

[20] S. Zhao, L. Cai, W. Chen, Y. He, and G. Du, "Self-heating and thermal network model for complementary FET," *IEEE Trans. Electron Devices*, vol. 69, no. 1, pp. 11–16, Jan. 2022, doi: 10.1109/TED.2021.3130010.

[21] (GaN Syst. Inc., Hsinchu, Taiwan). *GS-065-011-1-L 650V Enhancement Mode GaN Transistor*. Accessed: Apr. 27, 2020. [Online]. Available: https://gansystems.com/gan-transistors/gs-065-011-1-l/